





Cite this: *Chem. Commun.*, 2023, 59, 2469

Received 9th December 2022,
Accepted 26th January 2023

DOI: 10.1039/d2cc06707b

rsc.li/chemcomm

Photoswitchable semiconducting polymer dots for pattern encoding and superresolution imaging†

Zihan Yao,  ‡ Xiaodong Wang,  ‡ Jie Liu, Siyu Zhou, Zhe Zhang, Shuwen He, Jing Liu, Changfeng Wu  * and Xiaofeng Fang  *

Two photoswitchable semiconducting polymers were synthesized by covalently incorporating photochromic dithienylethene (DTE) into the main chains. Small size polymer dots (Pdots) were prepared and showed dynamic photoswitching upon alternate light irradiation. By virtue of the tunable photoswitching properties, effective pattern encoding and superresolution imaging with a resolution of up to about 30 nm were achieved.

Superresolution fluorescence microscopy provides a new quantitative means to study the interactions of subcellular components and biological processes in cells at the nanoscale.¹ These techniques require fluorescent probes with high brightness, strong photostability, and good biocompatibility.² In particular, the most common is single molecule localization microscopy (SMLM), such as photoactivated localization microscopy (PALM)³ and stochastic optical reconstruction microscopy (STORM),⁴ which can image a single fluorescent molecule, based on the photoswitching characteristics of the fluorescent probes, to precisely localize the distribution of fluorescence signals.⁵ However, the performance of SMLM imaging is dependent on fluorescent probes. Though fluorescent proteins have been used in SMLM technology, poor photostability, large size, and complex expression processes are non-negligible.⁶ Small molecule dyes based on rhodamines,⁷ spiropyran^{8,9} and DTE derivatives,^{10,11} which can switch the fluorescence on-off, have great potential advantages in SMLM due to their convenient preparation, small sizes, and tuneable photophysical properties.¹² Among them, DTE derivatives exhibit unique bistability, excellent fatigue resistance and high sensitivity,

and have broad applications in superresolution imaging^{13,14} and single-molecule junctions¹⁵ and so on. In addition, luminescent materials responsive to light stimuli also have great potential in information encryption, anti-counterfeiting and biosensors.^{16,17}

However, most small molecules as chromophores face the intrinsic challenges of low absorptivity and poor photostability. In contrast, Pdots prepared by π conjugated polymers demonstrate high brightness, strong photostability and fast transition rates and have recently achieved tremendous success in bioimaging, biosensing, theranostics,^{18,19} etc. In particular, in superresolution imaging, such as superresolution optical fluctuation imaging (SOFI)²⁰ and stimulated emission depletion microscopy (STED),²¹ Pdots show great promise for precisely revealing subcellular structures and dynamic interactions with an improved degree of detail and signal-to-background ratio.^{22,23} However, the spatial resolution can only be enhanced to about 70–150 nm in these two methods. STORM imaging can achieve a higher spatial resolution at the expense of the temporal resolution. There are a few photoswitchable Pdots prepared by physical doping and side-chain modification photochromic dyes have been reported for single cell sorting,²⁴ colour-tuneable illuminants,²⁵ and anticounterfeiting applications,²⁶ which in theory may also be applied to STORM imaging.

In this contribution, we synthesized two photoswitchable semiconducting polymers, DTE-PFBT and DTE-PFDTBT, by covalently incorporating photochromic DTE into the main chains. Detailed synthesis and characterizations are shown in Scheme 1 and the ESI.† Compared to physical doping methods and side-chain modification, main-chain functionalization has higher energy transfer efficiency.^{25,27} Pdots were prepared by modified nanoprecipitation following our previous works.²⁸ They maintained the reversible photoswitching properties upon alternate UV and visible light (Vis) irradiation. Apart from an obvious fluorescence switch, there were also significant chrominance changes. Fluorescence and colorimetric field dynamic pattern encoding was accomplished by light irradiation. Owing to the prominent brightness and photoswitching of the Pdots, STORM imaging with a ten-fold enhancement in spatial resolution to about 30 nm was possible.

Guangdong Provincial Key Laboratory of Advanced Biomaterials, Department of Biomedical Engineering, Southern University of Science and Technology, Shenzhen, Guangdong 518055, China. E-mail: jiangxf@sustech.edu.cn, wucf@sustech.edu.cn

† Electronic supplementary information (ESI) available: The details of the experimental methods, additional data including TEM images, optical spectra, the chemical structures of the polymers, DLS, and fluorescence images. See DOI: <https://doi.org/10.1039/d2cc06707b>

‡ These authors contributed equally to this work.



Scheme 1 (a) Synthesis routes of the open-ring DTE-PFBT and DTE-PFDTBT. (b) Schematic illustration of the photoswitching mechanism and applications in pattern encoding and STORM imaging.

The size of the DTE-PFBT Pdts (12 nm) was determined by dynamic light scattering (DLS) with a narrow particle size distribution (Fig. 1a). Well-dispersed spheres were found by transmission electron microscopy (TEM) and the size distribution was also consistent with the DLS result (Fig. 1b). The size and morphology of the DTE-PFDTBT Pdts are similar to those of DTE-PFBT Pdts (Fig. S6, ESI†). In addition, both have good colloidal stability with zeta potentials of -28.8 mV and -30.9 mV, respectively. No significant aggregation was observed within a month (Fig. S7, ESI†). The DTE unit can experience transition between open and closed isomers under UV or Vis irradiation (Fig. S8, ESI†); the corresponding absorption and fluorescence spectra of both the open and closed isomers were measured under alternate 365 nm and 620 nm irradiation (Fig. 1c and d). Upon irradiation of the DTE-PFBT Pdot solution at 365 nm, the absorption band at 620 nm gradually increased and reached the photostationary state at 60 s (Fig. S9, ESI†), accompanied by a colour change from yellow to pale green. This absorption band is attributed to the increment of conjugation induced by light isomerization. At the same time, the emission at 536 nm was quickly quenched under irradiation and the quantum yields decreased from 8.8% to 0.1%. After irradiation at 620 nm, both the absorption and fluorescence recovered to their original states. There were also significant absorption and fluorescence changes for the DTE-PFDTBT Pdts under the same light irradiation. The absorption at 650 nm gradually increased and the emission at 633 nm was quenched, accompanied by a decrease in the quantum yield from 6.7% to 0.9% under UV irradiation (Fig. S10, ESI†). The two photoswitchable Pdts also exhibited good reversibility and outstanding fatigue resistance during more than 6 repetitive cycles of alternate irradiation at 365 nm and 620 nm (Fig. 1e and Fig. S11–S12, ESI†). In addition, the Pdts showed good photostability; the fluorescence intensities were nearly unchanged under continuous excitation for 30 minutes (Fig. 1f). Thus, the DTE-PFBT and DTE-PFDTBT Pdts demonstrated good photoswitching ability, outstanding fatigue resistance, and excellent photostability, which make them good fluorescent probe candidates.



Fig. 1 Particle size and morphology of DTE-PFBT Pdts measured by DLS (a) and TEM (b). (c) The absorption and (d) fluorescence spectra of Pdot solutions under 365 nm (2 mW cm^{-2}) and 620 nm (50 mW cm^{-2}) irradiation. Insets: Pictures of the colour and fluorescence changes upon light irradiation. (e) Absorbance (620 nm) and corresponding fluorescence (536 nm) changes of DTE-PFBT Pdts during repetitive and alternate irradiation. (f) Photostability of Pdts under continuous excitation. I/I_0 is the ratio of the fluorescence intensity under irradiation to the initial fluorescence intensity.

Because of their versatile optical properties, we demonstrated their use for dual field dynamic encoding. As a proof of principle exhibition, the number “8” was written on paper with Pdot solution (Fig. 2a–i, ii). In the initial state, both numbers can be visually read in the bright fluorescence mode. After UV irradiation for 5 s, the time-dependency of the fluorescence for both numbers became distinct. At the same time, the colour changed from yellow and pink to green and red, respectively. The reflection spectra demonstrated that absorption in the visible area significantly increased (Fig. 2b, 2c). What is more, both the fluorescence and colour can be recovered to their initial state under irradiation at 620 nm, which is consistent with their solution spectral results. Therefore, the two photoswitchable Pdts can be used for dual field dynamic encoding. In addition, the Pdot solutions are compatible with commercial inkjet printers and can be directly put into ink cartridges.²⁹ These features suggest that the two photoswitchable Pdts have great potential for application.

In order to enrich the variety of optical encoding, we also prepared PFBT and PFDTBT Pdts lacking the photoswitchable unit by the same procedure. Fig. S13 (ESI†) shows the particle size and optical spectra of these Pdts. Under UV irradiation,



Fig. 2 (a) Fluorescence and colour pictures under UV and Vis irradiation of numbers painted with DTE-PFBT (i), DTE-PFDTBT (ii), PFBT except for segment 6 in DTE-PFBT (iii), PFDTBT except for segment 9 in DTE-PFDTBT (iv), PFBT mixed with DTE-PFDTBT (v), DTE-PFBT mixed with PFDTBT (vi), and DTE-PFBT mixed with DTE-PFDTBT (vii). (b–d) The reflectance spectra of DTE-PFBT, DTE-PFDTBT and the mixture of DTE-PFBT and DTE-PFDTBT Pdot solutions written on paper under alternate UV and Vis irradiation. Insets: Pictures of colour changes upon irradiation. (e–g) The fluorescence spectra of the PFBT mixed with DTE-PFDTBT, DTE-PFBT mixed with PFDTBT, and DTE-PFBT mixed with DTE-PFDTBT Pdot solutions under alternate UV and Vis irradiation, respectively. Insets: Fluorescence pictures under 365 nm by alternative irradiation.

the fluorescence of DTE-PFBT and DTE-PFDTBT faded and changes in reflectance can be observed by the naked eye, while PFBT and PFDTBT Pdots had no such effects. By combining photoswitchable and common Pdots with the same emission, one single stroke written with photoswitchable Pdots can dynamically change from the number “8” into “6” or “9” under UV irradiation (Fig. 2a-iii, iv). The quenched fluorescence originated from the photoisomerization of DTE moieties. The colour under Vis conditions also showed the same changes. The reflectance spectra of PFBT and PFDTBT Pdots remained unchanged (Fig. S14a and b, ESI†). In this way, the dual field dynamic encoding can greatly improve security. In addition to combining Pdots with the same emission, we also used orthogonal emission Pdots (PFBT mixed with DTE-PFDTBT or DTE-PFBT mixed with PFDTBT). By mixing photoswitchable and common Pdots with different emissions in proportion, we could obtain a new encoding mode. The fluorescence of the corresponding numbers changed from orange to yellow and red, respectively (Fig. 2a-v, vi). The changes in fluorescence and absorption are identical to the solution changes (Fig. 2e and f and Fig. S15, ESI†). The CIE chromaticity diagrams visually confirmed the corresponding fluorescence colour changes (Fig. S16, ESI†). Finally, we also directly combined the two photoswitchable Pdots and the fluorescence changed from orange to nothing (Fig. 2a-vii). The corresponding reflectance and fluorescence spectra also demonstrated the changes before and after UV irradiation. In conclusion, more complicated encryption can be achieved by permutation and combination of different Pdot solutions. Encoding modes not

only involved fluorescence and chrominance changes but also resulted in figure changes. Importantly, all changes are entirely reversible; both fluorescence and colorimetric field encoding can be recovered by 620 nm irradiation, and the encoding can be verified repeatedly. Thus, the use of photoswitchable Pdots in the fields of authentication and encryption is practical and promising.

The photoswitchable properties make DTE-PFBT and DTE-PFDTBT Pdots positive candidates for STORM imaging. We further proved the photoswitching feasibility by monitoring the fluorescence intensity changes under 365 nm, 405 nm, and 425 nm continuous irradiation (Fig. S17, ESI†). In order to rule out the effect of photobleaching, dissolved oxygen in the Pdot solution was removed by blowing it with argon gas. Under the same measurement conditions, all of the fluorescence intensities decreased significantly. These results indicate that ring-closed reactions can occur under continuous 405 nm irradiation. DTE moieties are covalently incorporated into the main chains, which enlarged their conjugation and visible region absorption, so the two Pdots can be used for visible light-driven photoswitching. In addition, the photoswitching performances of the two Pdots under 405 nm laser irradiation were also investigated with different optical power densities (Fig. S18, ESI†). As the power density increased, the fluorescence intensity exponentially decreased. The fluorescence intensity quickly decreased for the first 4 seconds. This is mainly due to the presence of multiple photoswitchable units. All of these results demonstrated that DTE-PFBT and DTE-PFDTBT Pdots possess excellent photoswitching properties and are compatible with common optical microscopy with a 405 nm laser for subsequent superresolution imaging.

We next employed the photoswitchable Pdots for subcellular labelling by antigen-antibody specific interaction. DTE-PFBT and DTE-PFDTBT Pdots were conjugated with streptavidin (SA) for immunofluorescence labelling; more detailed information can be found in the ESI.† The size distribution and surface zeta potential after bioconjugation were measured (Fig. S19, ESI†). The sizes of the Pdots-SA are about 5 nm larger in diameter compared with the original Pdots, which is consistent with the size of streptavidin. Because the carboxyl groups of the Pdots were bonded to streptavidin, an obvious increase in the zeta potential occurred, but it still remained negative (Fig. S19b and d, ESI†). Microtubules of BS-C-1 cells were labelled with the two photoswitchable Pdots and STORM imaging was performed on a lab-modified imaging system (Fig. 3). The microtubules imaged by widefield TIRF microscopy showed ambiguous edges (Fig. 3a and f), whereas the STORM reconstructed image had higher contrast and resolution (Fig. 3b and g). By analyzing the cross-sectional intensity profiles of microtubules in the images, the full width at half-maximum (FWHM) of the widefield image was calculated to be about 350 nm; however, *via* STORM imaging, the diameter of the microtubules was calculated to be as low as 32 nm (Fig. 3e and j), so there was a ten-fold enhancement in spatial resolution. These results reveal that photoswitchable Pdots have promising applications in the field of superresolution imaging based on single-molecule localization.



Fig. 3 Wide field fluorescence images of microtubules labelled with DTE-PFBT (a) and DTE-PFDTBT Pdots (f). (b), (g) STORM images corresponding to the same fields in (a) and (f), respectively. (c), (d), (h), and (i) Zoomed-in images of the regions marked with white rectangles in (a), (b), (f) and (g), respectively. (e), (j) Cross-sectional intensity profiles between the white arrows in (c) and (d), and (h) and (i), respectively.

In summary, we have developed two new types of photo-switchable polymers by covalently incorporating photochromic DTE into the main chains. The Pdots prepared by these polymers possess great fatigue-resistance and photoswitching properties. On the basis of the photophysical properties of the Pdots, fluorescence and colorimetric field dynamic encoding was achieved, uncovering potential for practical encryption applications. Finally, STORM imaging was performed, with a resolution of up to about 30 nm, which is higher than that of most reported superresolution imaging labelled by Pdots. Thus, these findings highlight the immense potential of Pdots for superresolution imaging applications.

This work was financially supported by the National Key R&D Program of China (No. 2020YFA0909000), the National Natural Science Foundation of China (No. 62235007, 22204070), the Shenzhen Science and Technology Program (No. KQTD20170810 111314625, JCYJ20210324115807021), the Shenzhen Bay Laboratory (SZBL2021080601002), and Guangdong Provincial Key Laboratory of Advanced Biomaterials (2022B1212010003).

Conflicts of interest

There are no conflicts to declare.

References

- 1 L. Wang, M. Tran, E. D'Este, J. Roberti, B. Koch, L. Xue and K. Johnsson, *Nat. Chem.*, 2020, **12**, 165–172.
- 2 Z. Yang, A. Sharma, J. Qi, X. Peng, D. Y. Lee, R. Hu, D. Lin, J. Qu and J. S. Kim, *Chem. Soc. Rev.*, 2016, **45**, 4651–4667.
- 3 E. Betzig, G. Patterson, R. Sougrat, S. Olenych, M. Davidson and H. Hess, *Science*, 2006, **313**, 1642–1645.
- 4 M. J. Rust, M. Bates and X. Zhuang, *Nat. Methods*, 2006, **3**, 793–795.
- 5 C. S. Wijesooriya, J. A. Peterson, P. Shrestha, E. J. Gehrmann, A. H. Winter and E. A. Smith, *Angew. Chem., Int. Ed.*, 2018, **57**, 12685–12689.
- 6 G. Matela, P. Gao, G. Guigas, A. F. Eckert, K. Nienhaus and G. U. Nienhaus, *Chem. Commun.*, 2017, **53**, 979–982.
- 7 S. N. Uno, M. Kamiya, A. Morozumi and Y. Urano, *Chem. Commun.*, 2017, **54**, 102–105.
- 8 Y. Zhang, K. H. Song, S. Tang, L. Ravelo, J. Cusido, C. Sun, H. F. Zhang and F. M. Raymo, *J. Am. Chem. Soc.*, 2018, **140**, 12741–12745.
- 9 Z. Ye, H. Yu, W. Yang, Y. Zheng, N. Li, H. Bian, Z. Wang, Q. Liu, Y. Song, M. Zhang and Y. Xiao, *J. Am. Chem. Soc.*, 2019, **141**, 6527–6536.
- 10 S. L. Gilat, S. H. Kawai and J. M. Lehn, *Chem. – Eur. J.*, 1995, **1**, 275–284.
- 11 S. H. Kawai, S. L. Gilat, R. Ponsinet and J. M. Lehn, *Chem. – Eur. J.*, 1995, **1**, 285–293.
- 12 L. Wang, M. S. Frei, A. Salim and K. Johnsson, *J. Am. Chem. Soc.*, 2019, **141**, 2770–2781.
- 13 N. A. Simeth, A. C. Kneutinger, R. Sterner and B. Konig, *Chem. Sci.*, 2017, **8**, 6474–6483.
- 14 C. Li, K. Xiong, Y. Chen, C. Fan, Y. L. Wang, H. Ye and M. Q. Zhu, *ACS Appl. Mater. Interfaces*, 2020, **12**, 27651–27662.
- 15 L. Hou, T. Leydecker, X. Zhang, W. Rehak, M. Herder, C. Cendra, S. Hecht, I. McCulloch, A. Salleo, E. Orgiu and P. Samori, *J. Am. Chem. Soc.*, 2020, **142**, 11050–11059.
- 16 J. Ao, X. Fang, X. Miao, J. Ling, H. Kang, S. Park, C. Wu and M. Ji, *Nat. Commun.*, 2021, **12**, 3089.
- 17 M. Irie, T. Fukaminato, K. Matsuda and S. Kobatake, *Chem. Rev.*, 2014, **114**, 12174–12277.
- 18 C. Wu and D. T. Chiu, *Angew. Chem., Int. Ed.*, 2013, **52**, 3086–3109.
- 19 J. Li and K. Pu, *Chem. Soc. Rev.*, 2019, **48**, 38–71.
- 20 Z. Liu, J. Liu, Z. Zhang, Z. Sun, X. Shao, J. Guo, L. Xi, Z. Yuan, X. Zhang, D. T. Chiu and C. Wu, *Nanoscale*, 2020, **12**, 7522–7526.
- 21 Y. Wu, H. Ruan, R. Zhao, Z. Dong, W. Li, X. Tang, J. Yuan and X. Fang, *Adv. Opt. Mater.*, 2018, **6**, 1800333.
- 22 Y. Wu, H. Ruan, Z. Dong, R. Zhao, J. Yu, X. Tang, X. Kou, X. Zhang, M. Wu, F. Luo, J. Yuan and X. Fang, *Anal. Chem.*, 2020, **92**, 12088–12096.
- 23 Y. Jiang, Q. Hu, H. Chen, J. Zhang, D. T. Chiu and J. McNeill, *Angew. Chem., Int. Ed.*, 2020, **59**, 16173–16180.
- 24 C. T. Kuo, A. M. Thompson, M. E. Gallina, F. Ye, E. S. Johnson, W. Sun, M. Zhao, J. Yu, I. C. Wu, B. Fujimoto, C. C. DuFort, M. A. Carlson, S. R. Hingorani, A. L. Paguirigan, J. P. Radich and D. T. Chiu, *Nat. Commun.*, 2016, **7**, 11468.
- 25 K. Watanabe, H. Hayasaka, T. Miyashita, K. Ueda and K. Akagi, *Adv. Funct. Mater.*, 2015, **25**, 2794–2806.
- 26 W. K. Tsai, Y. S. Lai, P. J. Tseng, C. H. Liao and Y. H. Chan, *ACS Appl. Mater. Interfaces*, 2017, **9**, 30918–30924.
- 27 Y. Osakada, L. Hanson and B. Cui, *Chem. Commun.*, 2012, **48**, 3285–3287.
- 28 X. Fang, B. Ju, Z. Liu, F. Wang, G. Xi, Z. Sun, H. Chen, C. Sui, M. Wang and C. Wu, *ChemBioChem*, 2019, **20**, 521–525.
- 29 K. Chang, Z. Liu, H. Chen, L. Sheng, S. X. Zhang, D. T. Chiu, S. Yin, C. Wu and W. Qin, *Small*, 2014, **10**, 4270–4275.